JOURNAL OF SOLID STATE CHEMISTRY 81, 152–164 (1989)

Paramagnetic Monitors (Mn^{2+}, Mn^{4+}, Fe^{3+}, and O_2^-) in the Solid-State Reaction Yielding $12CaO \cdot 7Al_2O_3$ and Other Aluminates

R. STÖßER

Department of Chemistry of the Humboldt-University, DDR-1080 Berlin, Bunsenstr. 1, German Democratic Republic

AND M. NOFZ, W. GEßNER, CH. SCHRÖTER, AND G. KRANZ

Central Institute of Inorganic Chemistry, Academy of Sciences of the German Democratic Republic, DDR-1199 Berlin, Adlershof, Rudower Chaussee 5, German Democratic Republic

Received May 18, 1988; in revised form February 22, 1989

$12CaO \cdot 7Al_2O_3$, $3CaO \cdot Al_2O_3$, and related phases were prepared starting from the respective mechanically activated oxides by solid-state reaction at 1200°C and identified by X-ray phase analysis. By means of EPR spectroscopy it was possible to characterize the state of mechanically and thermally activated starting materials using the signals of the paramagnetic species Mn^{2+}, Mn^{4+}, Fe^{3+}, and O_2^-. Structural changes which were caused by the solid-state reaction were clearly indicated by the EPR fine structure of Fe^{3+}. In addition the Fe^{3+} ions favor the solid-state reaction which is characterized by the diffusion of Ca^{2+} ions. The conclusions about the function of the paramagnetic centers in the starting materials and intermediates were confirmed by external pressure treatments of the samples in the GPa range. © 1989 Academic Press, Inc.

Introduction

The compound $12CaO \cdot 7Al_2O_3$ is of technical and scientific interest (*1–3*). It exhibits some unique physicochemical and structural properties. Commonly it is prepared in a solid-state reaction, but it can also exist in a glassy phase exhibiting interesting optical properties. The sensitivity of $12CaO \cdot 7Al_2O_3$ to external influences such as heat, pressure treatments, and reaction atmosphere makes it the object of several investigations. The structures of calcium aluminates were investigated and refined by means of diffraction methods (*4*). Recently Müller *et al.* (*2*) were able to detect further structural details in accordance with X-ray data published previously using ^{27}Al NMR.

The application of EPR spectroscopy to such a chemically and structurally active $CaO–Al_2O_3$ system (*5*) can yield valuable information about the structure and chemical properties of paramagnetic centers contained or generated in the starting materials and in the reaction mixture. By combination of EPR results with those of other spectroscopic, chemical, or mechanical methods (*6*), relevant assertions about the structure of the whole system can be obtained. Furthermore, by means of EPR it is possible to observe a high-temperature reaction by thermal quenching of samples at

0022-4596/89 $3.00

TABLE I

CHARACTERISTICS OF THE INVESTIGATED SAMPLES

Sample	Initial mixture	Time of heating (hr)	Milling process[a]	Results of X-ray phase analysis[b]						
				CaO	Al_2O_3	$Ca(OH)_2$	C_3A[c]	$C_{12}A_7$	CA	CA_2
I/1		5.5	A	+++	++	–	+++	+++	++(+)	++
I/2	$12CaO + 7Al_2O_3$	50.5	A	++(+)	+	(+)	++	++++	+++	+
I/3		14.5	B	+	–	–	(+)	+++++	+	–
II/1		5.5	A	+++	(+)	+	++	++	+(+)	+
II/2	$3CaO + 1Al_2O_3$	50.0	A	++	(+)	–	+++	+++	+(+)	+
II/3		14.5	B	–	–	–	+++++	+	(+)	–
III/1		5.5	A	++	+(+)	+(+)	++	++	++	+(+)
III/2	$5CaO + 3Al_2O_3$	50.5	A	+++	+	–	+	++(+)	+++	+
III/3		14.5	B	+	–	–	(+)	+++++	+	–

[a] A: ball crusher (agate balls), 15 min; B: vibrating mill (tungsten carbide disk), 2 min.

[b] Proportions between components in the mixture: fractions of the respective phase are valuated by the number of crosses.

[c] C and A stand for CaO and Al_2O_3 as commonly used in cement chemistry.

different stages of the reaction and comparing the results with those obtained by diffraction methods. One can deduce from the EPR findings the kind of structural changes done by means of paramagnetic species in the sample and it is expected that the paramagentic species favor the structural changes. Furthermore, from a mechanistic viewpoint the formation and stabilization of intermediate paramagnetic centers during the solid-state reaction is of special interest.

The starting compounds CaO and Al_2O_3 as well as the products (aluminates, essentially $12CaO \cdot 7Al_2O_3$) contain paramagnetic ions together with several defect centers. Both types of paramagnetic centers show a different sensitivity to the structural changes occurring during the solid-state reaction. The investigations of the solid-state reactions between CaO and Al_2O_3 at 1200°C were completed by EPR experiments carried out on glassy–crystalline and glassy samples obtained from quenched $12CaO \cdot 7Al_2O_3$ melts.

Experimental Procedures

Table I shows the composition of mixtures of starting materials, modes, and times of grinding, times of temperature treatments at 1200°C, and results of X-ray analysis (*7*). The temperature treatment was carried out in alumina crucibles. The conditions for the heat treatment of the starting materials CaO and Al_2O_3 were the same as for the solid-state reaction.

EPR spectra were obtained using a Varian E4 spectrometer operating in the temperature range $77 \leq T \leq 300$ K at microwave powers $0.1 \leq P_{MW} \leq 100$ mW.

Results and Discussion

Characterization of the Starting Materials by the Inherent Paramagnetic Centers

It seems to be customary first to characterize the properties of the paramagnetic centers contained in the starting materials because they are expected to react sensitively to changes of their environment produced by the individual steps of the solid-state reaction. Based on the EPR results obtained for CaO and Al_2O_3 the influence of thermal and mechanical pretreatment on the reactants must be discussed.

For the investigation of the component Al_2O_3 an α-Al_2O_3 charge was chosen, which contains Fe^{3+} on Al^{3+} sites as major impu-

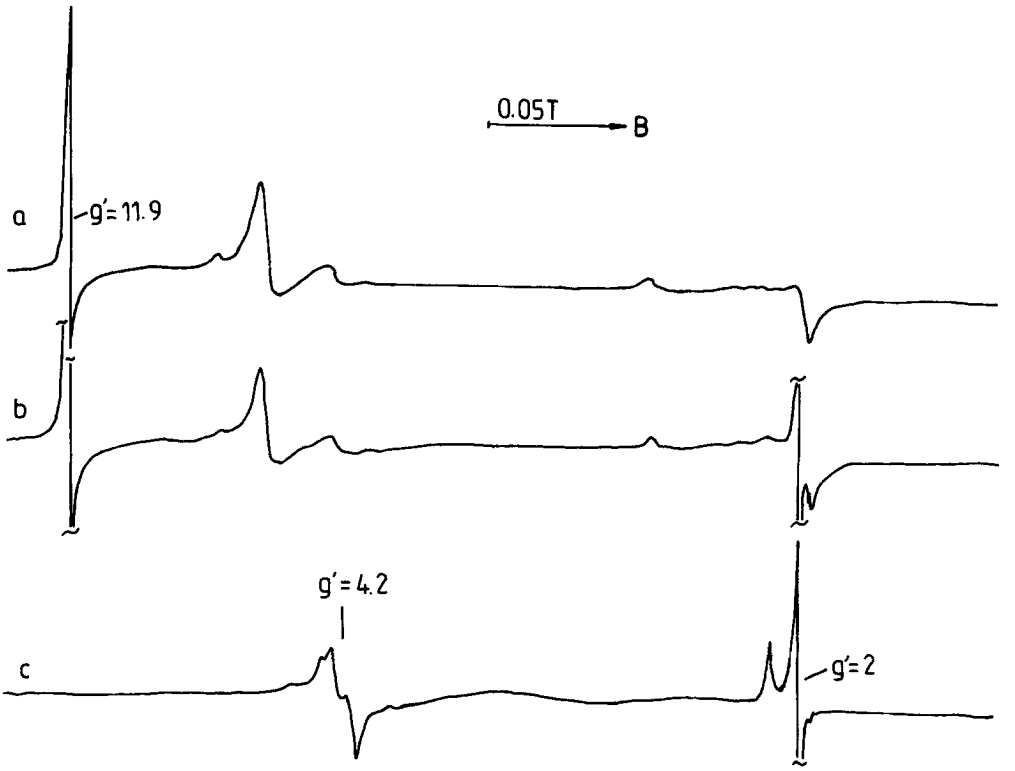

FIG. 1. EPR powder spectra of (a) Al_2O_3; (b) a ground mixture of ($12CaO + 7Al_2O_3$); (c) $12CaO \cdot 7Al_2O_3$.

rity and—as in almost all Al_2O_3 charges—a very small fraction of an autonomous Fe–O–Fe phase. The corresponding EPR spectrum is shown in Fig. 1a. Thermal treatments in the range between 700 and 1200°C lead to an increase of the Fe^{3+} EPR intensities of the signals with effective g-factors of $g' \sim 12$ and 5.3. This effect is in coincidence with the growing crystallinity of the sample and with the formation of rather more uniformly distorted sites for Fe^{3+} in Al_2O_3. Taking into account line width and line form functions of these signals they are well suited for an analytical characterization of alumina as shown during many investigations of the system α-Al_2O_3/Fe^{3+} (*8*). The EPR spectra and chemical analysis have shown that Al_2O_3 is the main Fe-source of the system under investigation. These Fe^{3+} ions mainly occupy sixfold coordinated sites in Al_2O_3. The CaO charge used as a starting material for the solid-state reaction is characterized by the EPR spectrum as shown in Fig. 2. This sample contains only traces of Fe^{3+} ($g' \sim 4.3$ and 2) but shows well-resolved spectra resulting from the hyperfine interaction of unpaired spins with ^{55}Mn and ^{53}Cr nuclei. The intensive line at $g' = 2.007$ represents the perpendicular component of an O_x^- center. A detailed analysis of the EPR spectra of the CaO used leads to the following conclusions: (i) Cr^{3+} centers with nearly cubic symmetry and $\bar{g} = 1.990$, $\bar{A} = 1.8$ mT are present in the sample. (ii) There is clear evidence of two Mn-species: $^{55}Mn(I)$ with $\bar{g} = 2.010$ and $\bar{A} = 8.7$ mT and $^{55}Mn(II)$ with $\bar{g} = 1.994$ and $\bar{A} = 7.7$ mT (see Fig. 2). From

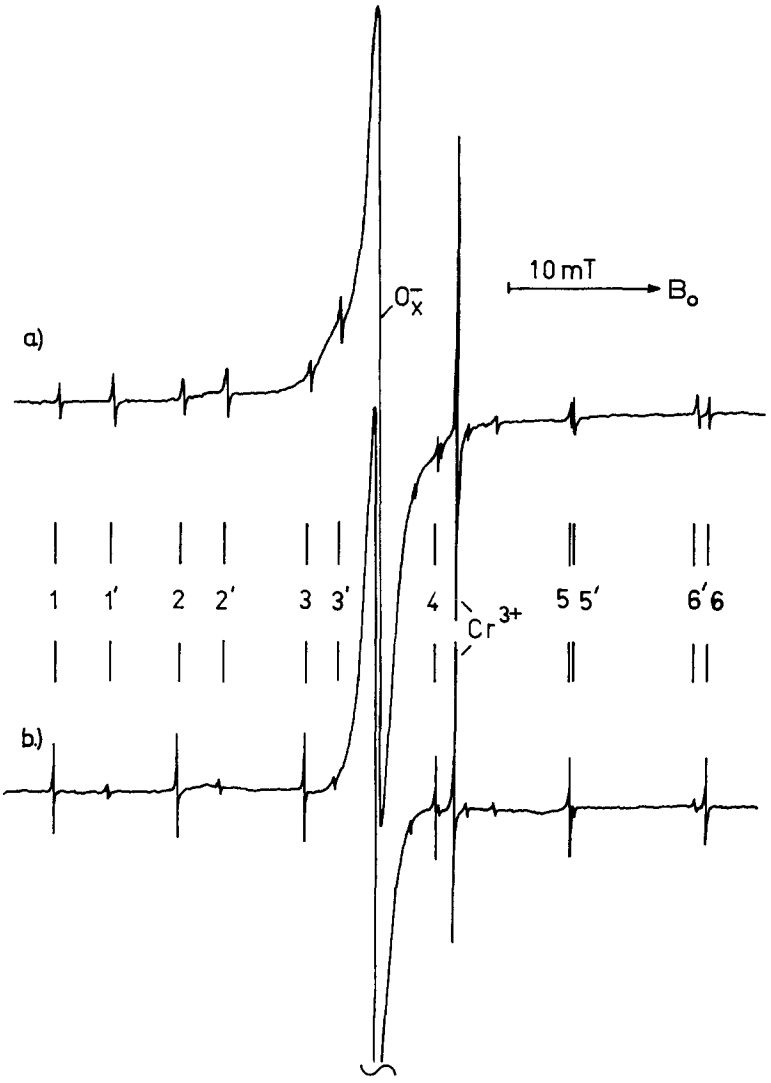

FIG. 2. Paramagnetic centers and ions in CaO used (a) before and (b) after temperature treatment at 1200°C for 20 hr.

both the g and A values and the saturation behavior of the signals one can deduce that species (I) represents Mn^{2+} on (mainly) cubic sites in CaO and species (II) is Mn^{4+} on tetragonally distorted sites (see (*9*)) charge compensated by an O^{x-} center. The Mn species (II) might also be explained by the assumption of an axial Mn^{2+} center in CaO perturbed by an adjacent F center (*10*). Examination of the g values favors the interpretation of a Mn^{4+} species as that center (see, e.g., (*11*)). Figure 3 shows the dependence of these signals (using the intensity ratios of the 6 hfs lines of species (I) (1 . . . 6) and (II) (1′ . . . 6′)) on the microwave power (P_{MW}) applied in the EPR experiment. At low P_{MW} (Fig. 3b) the intensity of species (II) exceeds that of (I). With in-

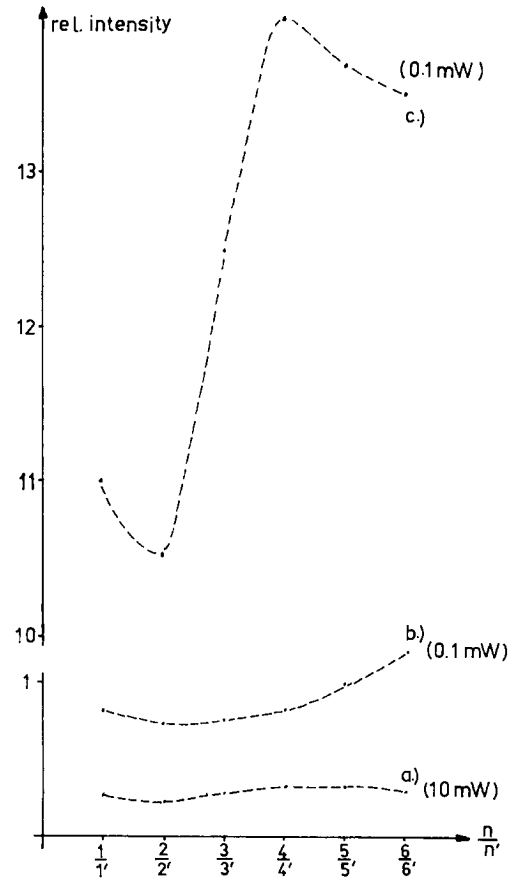

FIG. 3. Intensity ratios (1/1' . . . 6/6') for the six hfs lines of ^{55}Mn species I (1 . . . 6) and II (1' . . . 6') in CaO at (a) P_{MW} = 10 mW, (b) P_{MW} = 0.1 mW, and (c) after high-temperature treatment (1200°C for 20 hr) and P_{MW} = 0.1 mW.

creasing P_{MW} species (II) dominates the spectrum because the Mn^{2+} ions at cubic sites tend to saturate. Species (II) (Mn^{4+}) is characterized by a zero field splitting (zfs) in the range of 50 mT. This and the $^4F_{3/2}$ ground state are the prerequisites for a faster spin relaxation (Fig. 3a) of Mn species (II) compared to (I).

After a high-temperature treatment (1200°C for 20 hr) the intensity ratios 1/1' . . . 6/6' have increased rapidly and show an extremum (Fig. 3c). Thus not only the dominance of Mn^{2+} at cubic sites is reflected but also a lowering of species (II) intensity by increased zfs contributions is indicated. These findings imply that a certain amount of local imperfections in the CaO powder (contributing to the activation of this reactant) remain even after thermal treatment.

Some selected signal intensities of CaO, which was treated in a temperature range between 700 and 1200°C for 5.5 hr, are shown in Fig. 4, and the increasing intensities at higher temperatures ($T > 900$°C) are due to the dominance of Mn^{2+} species at cubic sites. The O_x^- and Cr^{3+} centers show extreme behavior in the temperature range between 800 and 1000°C. At higher temperatures these centers are characterized by rising intensities, also. For Cr^{3+} (Fig. 4a) in principle the same arguments are valid as for Mn^{2+}.

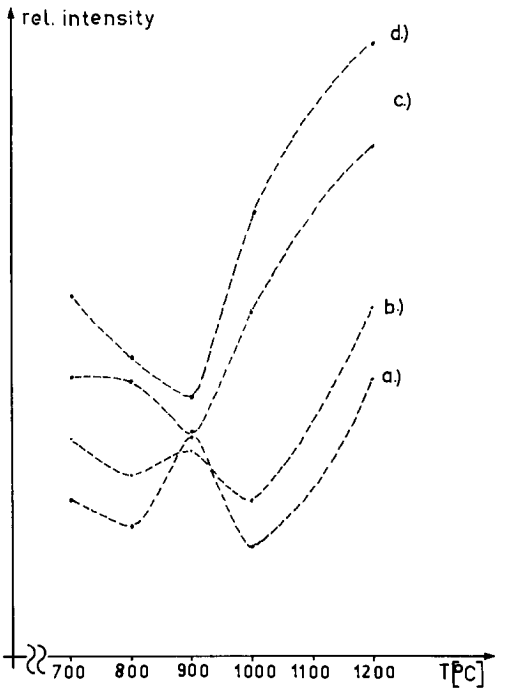

FIG. 4. Temperature dependence of the intensities for (a) Cr^{3+}, (b) O_x^-, (c) ratios 1/1', and (d) ratios 6/6' in CaO (see Fig. 3).

The observation of the intensity changes of the O_x^- and Mn(II) signals is a simple method to detect the activation of the starting materials in the grinding process. The significant decrease of their intensities (caused by chemical reaction as well as by line broadening) attests to the distortions of the environment of the ions induced mechanically. Equipped with the results discussed above we are able now to assign changes of the EPR spectra after the temperature treatment of the reaction mixtures either to changes of the starting materials themselves or to the formation of reaction products.

On the Progress of the Solid-State Reaction between CaO and Al_2O_3

Concerning a solid-state reaction between CaO and Al_2O_3 the following questions should be taken into consideration: (i) What kinds of elementary steps are involved in the reaction? (ii) How do the composition, the temperature/time relationship, and the mechanical pretreatment affect the yield and manifold of products? Identifying the crystalline phases in the reaction mixtures and estimating their amounts by means of X-ray diffraction (Table I) shows a dependence on the mechanical activation of the starting materials. Obviously the phase $3CaO \cdot Al_2O_3$ really plays an extraordinary role in this system. $3CaO \cdot Al_2O_3$ appears to be ubiquitous and represents the CaO-richest phase among all reaction products detected. For its subsequent reaction to $12CaO \cdot 7Al_2O_3$ diffusion of Al^{3+} is expected due to the stoichiometry. One conclusion from these experiments is that under the given conditions the diffusion of Ca^{2+} is favored which is in accordance with the different properties of the materials CaO and Al_2O_3. This corresponds to the observations of De Jonghe *et al.* (*12*) who examined the interactions of Al_2O_3 and a $CaO–Al_2O_3$ melt. It must be mentioned that the way of preparing and activating the reactants is important, as well; e.g., Hosono and Abe (*13*) used $CaCO_3$ as starting material.

Under the conditions of (i) restricted Ca^{2+} supply, (ii) intensive activation, and (iii) long-time temperature treatment, $12CaO \cdot 7Al_2O_3$ is preferably formed, whereas $3CaO \cdot Al_2O_3$ is favored even under moderate conditions (Table I).

It is presently our aim to show how EPR spectroscopy provides additional information about the progress of the reaction between CaO and Al_2O_3 in such a way that the intermediate steps can be clearly detected. Therefore we must study the spectral and intensity behavior of Fe^{3+}, which is an impurity of Al_2O_3, such as Mn^{2+}, Mn^{4+}, and O^- in CaO, as well as the formation of O_2^-, which is effectively stabilized in the reaction product $12CaO \cdot 7Al_2O_3$.

First, the EPR fine structure caused by Fe^{3+} in Al_2O_3 should be discussed. Concerning the investigation of the solid-state reaction between CaO and Al_2O_3 two questions are important: (i) Does Fe^{3+} serve as a monitor for the environment of Al^{3+} and (ii) does the solid-state reaction start preferably at or near the Fe^{3+} sites in the Al_2O_3 lattice? The EPR fine structure of Fe^{3+} caused by the zfs of the spin states is usually very sensitive to small changes of the symmetry of the Fe^{3+}/Al^{3+} sites. The zfs should therefore be a good indicator for the reaction induced change of the coordination number from 6 in Al_2O_3 to ultimate 4, e.g., in $12CaO \cdot 7Al_2O_3$.

A change of the intensity ratios of the fine structure of Fe^{3+} in Al_2O_3 is generally observed if the reaction proceeds for a certain time at 1200°C; i.e., the intensity at $g' \sim 5.12$ decreases more than that at $g' \sim 11$. Such a change of the intensity ratios can be seen more clearly if the mixture is ground in an agate mortar because here the activation of Al_2O_3 is mainly caused by the iron impurity and not be mechanical changes of the structure (in contrast to the samples ground

in a tungsten carbide vibration mill). The results obtained for Al_2O_3 doped with Fe^{3+} (*8, 14*) show that the intensity ratio of the resonance positions at $g' \sim 11$ and 5.12 depends on the actual Fe^{3+} content, on its distribution in the volume of the crystallites, and on the crystallinity of the sample. The greater decrease of the intensity of the signal at $g' \sim 5.12$ compared to that at $g' \sim 11$ is caused by the consumption of Al_2O_3 and by an enhanced attack of Ca^{2+} on Al_2O_3 in the region near the sites of Fe^{3+}, which changes the local symmetry and thus increases the distance between the iron ions. In contrast, the diffusion of Fe^{3+} into Al_2O_3 at 1300°C results in an increase and broadening of the $g' \sim 5.12$ resonance (compare (*8, 14*)) due to magnetic dipole–dipole interactions between these ions. The following explanation for the elemental processes of the reaction between CaO and Al_2O_3 could be given: The Al_2O_3 lattice is locally deformed and as a result of the Ca^{2+} attack the coordination sphere of the Fe^{3+} ions is changed. One can expect a change from FeO_6 to FeO_4 at least as determined for the Al^{3+} ions by X-ray analysis and NMR studies (*2, 4*).

As mentioned above the $3CaO \cdot Al_2O_3$ phase exists ubiquitously in all samples (see Table I) and the fine structure pattern caused by Fe^{3+} in this $3CaO \cdot Al_2O_3$ lattice (Fig. 5) is observed even in the case of the less efficient activation by mechanical pretreatment in the agate mortar. The spectrum in question represents a superposition of that for Fe^{3+} in $3CaO \cdot Al_2O_3$ and for Fe^{3+} in Al_2O_3 (compare Fig. 5) not yet transformed during the reaction. Based on these findings one can assume that under such experimental conditions not only is the formation of the compound $3CaO \cdot Al_2O_3$ favored but its indication by the well-resolved Fe^{3+} fine structure is also advantageous with respect to the X-ray method. Additionally it should be underlined that an ordered phase is not necessary to detect the formation of $3CaO \cdot Al_2O_3$ by means of EPR.

If the CaO/Al_2O_3 ratio is decreased (e.g., 12/7; compare I/1–I/3 in Table I) a relatively higher pool of Fe^{3+} is available. From the analysis of the corresponding EPR spectra it follows that the Fe^{3+} is mainly incorporated into $3CaO \cdot Al_2O_3$ and to a lower extent into the coexisting $12CaO \cdot 7Al_2O_3$. The corresponding EPR spectra show that Fe^{3+} is found to a greater extent in $3CaO \cdot Al_2O_3$ than in $12CaO \cdot 7Al_2O_3$. If the amount of $12CaO \cdot 7Al_2O_3$ is increased, e.g., as a result of the pretreatment, the available Fe^{3+} is only partially incorporated into the $12CaO \cdot 7Al_2O_3$ lattice but forms an autonomous Fe–O phase giving broad EPR lines in the region $3 > g' > 2$ (Fig. 5). Obviously the $12CaO \cdot 7Al_2O_3$ structure is not able to incorporate as much Fe^{3+} as $3CaO \cdot Al_2O_3$ and related phases. Otherwise the spectra in Fig. 5 show some similarities for the fine structure pattern of Fe^{3+} incorporated in $3CaO \cdot Al_2O_3$, $12CaO \cdot 7Al_2O_3$, and "$5CaO \cdot 3Al_2O_3$." But, especially for $12CaO \cdot 7Al_2O_3/Fe^{3+}$, broader lines for the low field transitions are observed. They indicate (i) that there are magnetic interactions between the Fe^{3+} ions and (ii) that there is a greater variety of the distortions of the coordination polyhedra in $12CaO \cdot 7Al_2O_3/Fe^{3+}$ than in the sample containing $3CaO \cdot Al_2O_3/Fe^{3+}$.

For the analysis of the Fe^{3+} fine structure in this system it is advantageous that the signals from the reactants and those of the intermediates and products (Fig. 1) show no superposition. The CaO used for the investigations contains traces of Mn^{2+} and in the magnetic field around $g' = 2$ the hfs of Mn^{2+} can be observed. Figure 2 indicates unequivocally the existence of two Mn species. Due to its structure, species II shows a greater reactivity (see (*9, 11*)). The intensity of the EPR signal of species II is actually smaller than that of I by the grinding process of the mixture of starting materials

FIG. 5. Low field region (0–0.2 T) of the Fe^{3+} fine structure of the starting mixtures (upper curves) and the reaction mixtures. Left and right side: Pretreatment as A and B, respectively (compare Table 1).

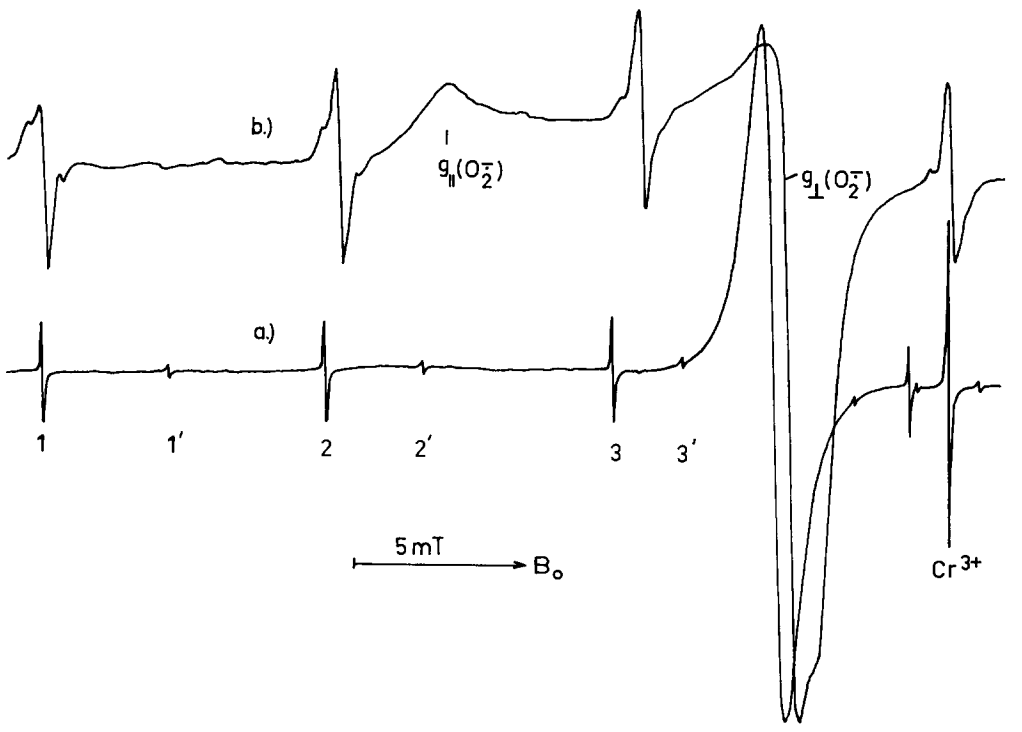

FIG. 6. Part of the $g \sim 2$ region for (a) CaO after heat treatment at 1200°C for 20 hr, and (b) ($12CaO + 7Al_2O_3$) mixture after 50 hr temperature treatment at 1200°C (compare Table 1, sample I/2).

as well as by the solid-state reaction. Furthermore, the incorporation of Mn^{2+} into the arising $12CaO \cdot 7Al_2O_3$ phase is observable by the superposition of a new Mn^{2+} species ($A = 8.9$ mT) and disappearance of Cr^{3+} (Fig. 6).

Comparing the results of the temperature treatment of CaO itself and of the mixture of CaO and Al_2O_3, respectively one can see that there is a difference between the behavior of species I and II. The changes of the intensity of Mn^{x+} species I and II in CaO are significantly smaller (about 10^{-3}) than in the mixture of oxides. The efficiency of the solid-state reaction is essentially dependent on both grinding and temperature treatments (compare I/1 with I/3 of Table I). As one can see in Table I the desired phase arises from the oxides with increasing activation and time of temperature treatment. Repeated grinding and temperature treatment gives a greater yield of the desired products. However, it was one aim of the investigations described here to get an indication for the structural changes at the beginning and during the solid-state reaction between CaO and Al_2O_3.

As the Mn^{2+} and Mn^{4+} in CaO indicate the reactions between the starting materials, so does the Fe^{3+} in Al_2O_3. The intensities of the Fe^{3+} peaks at $g' \sim 12$ and 5.3 (*8*) represent the percentage of Al_2O_3 in the mixture of reaction products in a good approximation.

The consumption of reactants during the progress of the solid-state reaction detected by the decrease of the intensities of Mn^{2+} and Fe^{3+} signals in the EPR spectra corresponds with the results of X-ray analysis

(see Table I). Both ions will be included in the reaction products obviously. Although the reaction products contain more than one component, X-ray phase analysis allows the identification of nearly all peaks and thus all of the components in the mixture of reaction products. By means of EPR spectroscopy the phase $12CaO \cdot 7Al_2O_3$ can be detected additionally due to the characteristic fine structure of Fe^{3+} as well as the Mn^{2+} hfs and the intensive O_2^- signal. It is to be expected that both starting oxides contain small entities of Fe^{3+}—possibly as some sort of an autonomous Fe–O–Fe phase—which cannot easily be detected. Alumina contains Fe^{3+} on Al^{3+} sites within the lattice; thus, these ferric ions will be sixfold coordinated. During the reaction between Al_2O_3 and CaO the coordination of Fe^{3+} ions (assuming that Fe^{3+} substitutes Al^{3+}, as widely accepted) changes. Simultaneously Fe^{3+} out of an above-mentioned oxidic Fe–O phase could be incorporated into Al_2O_3 or $12CaO \cdot 7Al_2O_3$ by diffusion. At the temperature chosen this process is of no importance because of its relatively small efficiency. It becomes essential at 1350°C and by a long-term temperature (*8, 14*). Nevertheless it is not easy to determine the fraction of Al_2O_3 quantitatively because the temperature treatment of pure Al_2O_3 at 1200°C increases the crystallinity and therefore the intensity of the EPR signals at $g' \sim 12$ and 5.3. However, the correspondence between the percentage of Al_2O_3 in the reaction products determined by EPR spectroscopy on the one hand and by X-ray phase analysis on the other hand indicates that Al_2O_3 reacts chemically and that at the beginning of the reaction the lattice will be disturbed in the surface region of the cyrstallites (instead of perfection taking place). Thus the EPR signals with $g' \sim 6$ can be used for the indication of the proceeding reaction because the reaction products do not show any signal in that region. The change of the coordination number of Al^{3+} was indicated by the Fe^{3+} signals of the corresponding or substituting impurity with $3.5 < g' < 4.9$ (Fig. 5) and by the decrease of the signals with $g' \sim 12$ and 5.3. The signal with $3.5 < g' < 4.9$ can be assigned to Fe^{3+} species with an axially ($D > 0.2$ cm^{-1}) or orthorhombically distorted surrounding. Different distortions of $[Fe^{3+}O_x]$ polyhedra are possible within the $12CaO \cdot 7Al_2O_3$ structure. The Fe^{3+} fine structure with $g' \sim 4.4, 4.0 \ldots$ and the transitions at $g' \sim 4.28$ (Fig. 5) are caused by tetragonal and orthorhombic distortions of the Fe^{3+} coordination polyhedron. It is surprising and may be estimated as further proof for the incorporation of Fe^+ into the structure that in contrast to other Fe^{3+} containing compounds the intensity at $g' \sim 4.28$ does not in any way dominate the spectrum.

The sensitivity of Fe^{3+} coordination polyhedra and its nearest neighbors to small structural changes is also clearly demonstrated by applying external pressure (up to 400 T per 0.79 cm^2 (*5*)) on $12CaO \cdot 7Al_2O_3$ powders: The intensity at $g' \sim 4.28$ increases in the course of this treatment at the expense of the intensity of the other components of the fine structure. At the same time, unexpected from a chemist's viewpoint, the spectrum and the concentration of O_2^- remains mainly unchanged. Consequently the pressure induced structural changes originate at the Fe^{3+} sites in the lattice (as does the chemical reaction also), but even a high-pressure treatment is not able to destroy the overall structure of the cement component $12CaO \cdot 7Al_2O_3$.

On Some Pecularities of the $12CaO \cdot 7Al_2O_3$ Structure

The investigation of the product $12CaO \cdot 7Al_2O_3$ by means of EPR spectroscopy resulted in the detection of a typical O_2^- signal with parameters $g_\parallel = 2.075$ and $g_\perp = 2.009$. The distinct g anisotropy in addition to the characteristic dependence on temperature

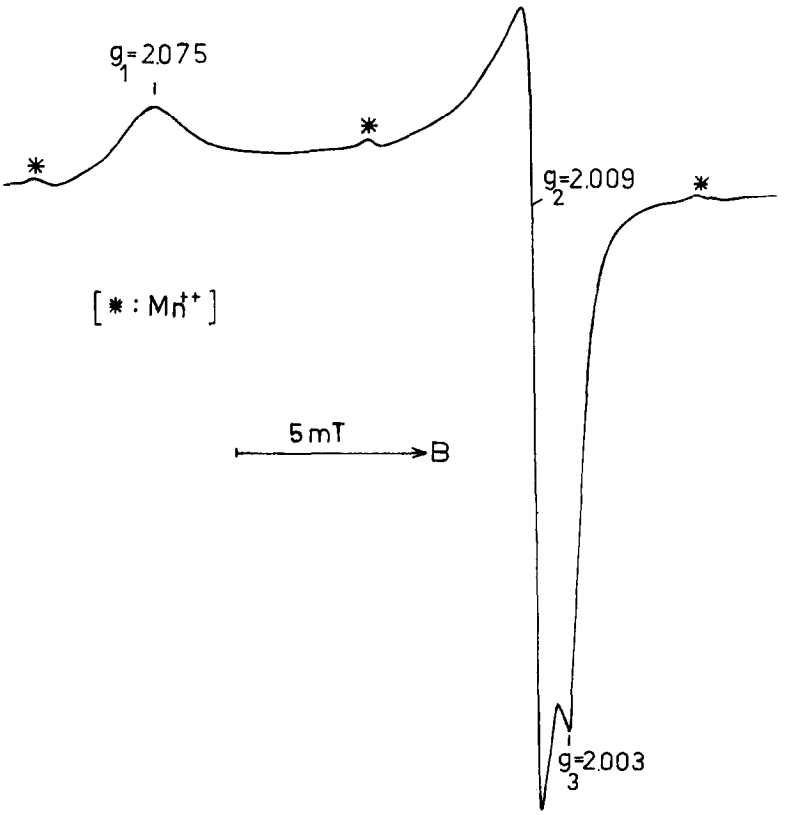

FIG. 7. EPR spectrum of O_2^- in $12CaO \cdot 7Al_2O_3$ at 77 K.

(i.e., the reversible activation of motional averaging of the g anisotropy (*15*) in the temperature range between 77 and 300 K) as well as the small saturation tendency (and not at the least the agreement of the g components found with those published in the literature (*13, 16*)) confirm the interpretation of the EPR signals given (Fig. 7). The observed restricted motion of O_2^- and selected chemical experiments (spare hydratation, interaction of a solution of nitroxide radicals in water with the surface) lead to the conclusion that these centers are existing in the volume of the $12CaO \cdot 7Al_2O_3$ powder. The concentration of O_2^- is of about 10^{19} spins/g and can unambigously be increased by a temperature treatment (900°C) within an oxygen atmosphere or decreased in a nitrogen atmosphere. It is an interesting fact that the reactive species O_2^- is stabilized in the volume of the crystallites during the quenching process of the reaction mixture from 1200 to 25°C and not at the surface as often detected for oxides (*16, 17*).

A second surprising result is the observation that the O_2^- concentration is only slightly decreased after a heat treatment for more than 100 hr at temperatures in the range between 700 and 1200°C. Bearing in mind these findings, one can understand that the detectable amount of O_2^- increases with growing content of $12CaO \cdot 7Al_2O_3$ in the mixture of reaction products. The yield of the superoxide anion also seems to profit from the transformation of the Mn species

(II) into (I) during the solid-state reaction. From the experimental facts one can conclude that the formation and stabilization of the O_2^- species is favored by the structure of the $12CaO \cdot 7Al_2O_3$ lattice (*1, 3, 4*). Under electronic aspects the system $12CaO \cdot 7Al_2O_3$ represents a structure with deep traps, acting therefore as a very effective quencher for electronic defects. It was impossible indeed to stabilize defects other than those of O_2^- in $12CaO \cdot 7Al_2O_3/O_2^-$ after irradiation with γ-rays even at low temperatures or by mechanic activation. The conclusions made here on the basis of spectroscopic data are in agreement with the observation of Brisi and Borlera (*1*). They found that a cold dissolution of $12CaO \cdot 7Al_2O_3$ in diluted hydrochloric or perchloric acid shows a typical peroxidic behavior. The resulting H_2O_2 of this solution was quantitatively determined by means of titration. A direct proof of O_2^-, e.g., using EPR, has been done (*3, 13*).

The lattice of $12CaO \cdot 7Al_2O_3$ consists of $[Al^{(4)}O_2]$ and $[Al^{(4)}O_{2.5}]^-$ units and additionally includes cavities in the unit cell out of which 8% are filled with oxygen atoms. There should be a connection between the favored stabilization of O_2^- on the one hand and side the two oxygen atoms on the other, which are additionally included in the unit cell ("excess oxygen"), as well as the possiblity of incorporating O_2, H_2O, or OH^- into the cavities of the structure.

Comparing the EPR spectra of $12CaO \cdot 7Al_2O_3$ and of sample II/3 (with stoichiometric composition of $3CaO \cdot Al_2O_3$) some differences shall be stated. Some types of O_2^--like defects ($g_\parallel = 2.074$; $g_\perp = 2.009$) could be detected in rather small concentrations (~1/100 or that in $12CaO \cdot 7Al_2O_3$) as observable in many other inorganic materials (especially oxides). These signals are possibly caused by $12CaO \cdot 7Al_2O_3/O_2$ impurities contained in this sample as detected by means of X-ray analysis (Table I). The structure of $3CaO \cdot Al_2O_3$ does not favor the formation and stabilization of O_2^-. Excess oxygen atoms are not included regularly in the crystallites. In principle rather small cavities also exist in the structure of $3CaO \cdot Al_2O_3$ but they are situated within rings of $[Al^{(4)}O_3]$ units and Ca–O distances are shorter than in $12CaO \cdot 7Al_2O_3$.

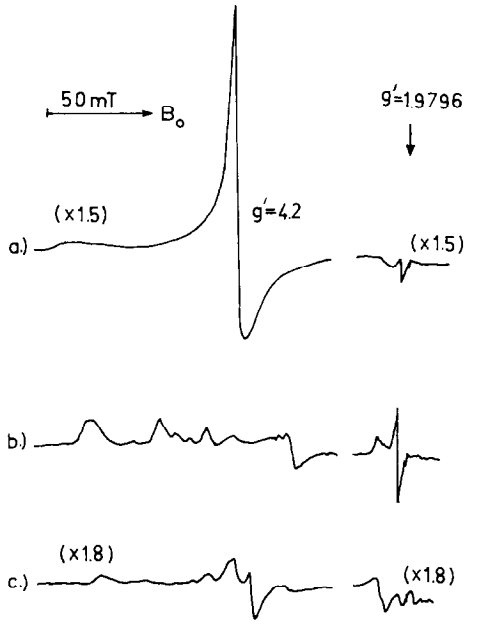

FIG. 8. EPR of (a) glassy and (b,c) crystalline $12CaO \cdot 7Al_2O_3$ at 77 K. The starting materials of (a) and (b) were milled in an agate mortar and those of (c) in a tungsten carbide vibration mill (see (*5*)).

An additional proof for the stabilization of O_2^- in the cavities of $12CaO \cdot 7Al_2O_3$ is based on the investigation of the corresponding glassy phase. In such a glass, formed by quenching a melt with the composition of $12CaO \cdot 7Al_2O_3$, an EPR spectrum is observed with the typical pattern of Fe^{3+} impurities in glasses (Fig. 8a). Only traces of O_2^- species can be detected in the $g \sim 2$ region. The much higher O_2^- concentration observed by (*13*) can be explained by the fact that crystalline domains were present in these samples. Such an elucidation would agree with the conclusions of Morikawa *et al.* (*18*). On the basis of scat-

tering data they pointed out that a so-called $12CaO \cdot 7Al_2O_3$ glass is better described by a modified $5CaO \cdot 3Al_2O_3$ structure than by a distorted $12CaO \cdot 7Al_2O_3$ one. This and the increase of density due to the vanishing cavities by the transition to the glassy state could explain the low concentration of O_2^- in this glass. As shown in Figs. 8b and 8c the O_2^- concentration in the devitrificated $12CaO \cdot 7Al_2O_3$ glass is quite high but does not reach the concentration range observed for samples obtained by solid-state reaction.

References

1. C. Brisi and M. L. Borlera, *Il Cemento* **80,** 155 (1983); M. L. Borlera and C. Brisi, *Il Cemento* **81,** 13 (1984).
2. D. Müller, W. Gessner, A. Samoson, E. Lippmaa, and G. Scheler, *Polyhedron* **5,** 779 (1986).
3. R. Stösser, M. Nofz, and W. Gessner, *Z. Chem.* **27,** 111 (1987); R. Stösser, M. Nofz, and W. Gessner, *Z. Chem.* **27,** 189 (1987).
4. H. Bartl and Th. Scheller, *Neues Jahrb. Mineral. Monatsh.*, 547 (1970).
5. R. Stösser, M. Nofz, and R. Lück, *Exp. Techn. Phys.* **36,** 327 (1988).
6. R. Stösser, A. Rericha, and R. Lück, "High Pressure in Geosciences and Material Synthesis" (M. Vollstädt, Ed.), "Proc. of the XXV Annual Meeting of the European High Pressure Research Group, Potsdam, GDR, August, 1987." pp. 252–255. Akademie-Verlag, Berlin (1988).
7. Ch. Schröter, G. Kranz, and J. Wiegmann, *Silikattechnik* **36,** 108 (1985).
8. R. Stösser, R. Brenneis, and I. Ebert, *J. Mater. Sci.*, in press; R. Brenneis, Thesis, Academy of Sciences of the GDR (1988).
9. R. Lück, R. Stösser, and F. Von Lampe, *in* "Proceedings, EPR-Tagung, Physikal. Gesellschaft d. DDR, Rohrbach," p. 53 (1986).
10. H. S. Murrieta, J. O. Rubio, M. G. Aguilar, and J. Garciasole, *J. Phys. C: Solid State Phys.* **16,** 1945 (1983).
11. J. J. Davies, S. R. P. Smith, and J. E. Wertz, *Phys. Rev.* **178,** 608 (1969).
12. L. C. De Jonghe, H. Schmid, and M. Chang, preprint, submitted for publication (1983).
13. H. Hosono and Y. Abe, *Inorg. Chem.* **26,** 1192 (1987).
14. R. S. De Biasi and D. C. S. Rodrigues, *J. Mater. Sci. Lett.* **2,** 210 (1983).
15. S. Schlick and L. Kevan, *J. Phys. Chem.* **83,** 3424 (1979); D. Suryanarayana, L. Kevan, and S. Schlick, *J. Amer. Chem. Soc.* **104,** 668 (1982).
16. T. Baba and K. Ikeda, *J. Phys. Soc. (Japan)* **50,** 217 (1981).
17. R. Stösser and H. J. Lunk, *Dokl. Akad. Nauk USSR* **297,** 422 (1987).
18. H. Morikawa, F. Marumo, T. Koyama, M. Yamane, and A. Oyobe, *J. Non-Cryst. Solids* **56,** 355 (1983).